Published in final edited form as:
J Bone Miner Res. 2012 February ; 27(2): 263–272. doi:10.1002/jbmr.562.

Individual Trabecula Segmentation (ITS)-Based Morphological Analyses and Micro Finite Element Analysis of HR-pQCT Images Discriminate Postmenopausal Fragility Fractures Independent of DXA Measurements

X. Sherry Liu[1,*], **Emily M. Stein**[1,*], **Bin Zhou**[2], **Chiyuan A. Zhang**[1], **Thomas L. Nickolas**[1], **Adi Cohen**[1], **Valerie Thomas**[1], **Donald J. McMahon**[1], **Felicia Cosman**[2], **Jeri Nieves**[2], **Elizabeth Shane**[1,+], and **X. Edward Guo**[3,+]

[1]Division of Endocrinology, Department of Medicine, College of Physicians and Surgeons, Columbia University New York, New York, U.S.A.

[2]Helen Hayes Hospital, Clinical Research Center, West Haverstraw, New York, U.S.A.

[3]Bone Bioengineering Laboratory, Department of Biomedical Engineering, Columbia University New York, New York, U.S.A.

Abstract

Osteoporosis is typically diagnosed by dual energy x-ray absorptiometry (DXA) measurements of areal bone mineral density (aBMD). Emerging technologies, such as high-resolution peripheral quantitative computed tomography (HR-pQCT), may increase the diagnostic accuracy of DXA and enhance our mechanistic understanding of decreased bone strength in osteoporosis. Women with (n=68) and without (n=101) a history of postmenopausal fragility fracture had aBMD measured by DXA, trabecular plate and rod microarchitecture measured by HR-pQCT image-based individual trabeculae segmentation (ITS) analysis, and whole bone and trabecular bone stiffness by micro finite element analysis (μFEA) of HR-pQCT images at the radius and tibia. DXA T-scores were similar in women with and without fractures at the spine, hip and 1/3 radius, but lower in fracture subjects at the ultradistal radius. Trabecular microarchitecture of fracture subjects was characterized by preferential reductions in trabecular plate bone volume, number, and

[+]**Co-Corresponding Authors**: X. Edward Guo, Ph.D. Columbia University Department of Biomedical Engineering 351 Engineering Terrace, Mail Code 8904 1210 Amsterdam Avenue New York, NY 10027, U.S.A. ed.guo@columbia.edu Telephone: 212-854-6196 Fax: 212-854-8725. [+]Elizabeth Shane, M.D. Columbia University College of Physicians and Surgeons 630 West 168th Street PH8 West 864 New York, NY 10032, U.S.A. es54@columbia.edu Telephone: 212-305-6289 Fax: 212-305-6486.
(xl2014@columbia.edu)
(es2029@columbia.edu)
(bz2159@columbia.edu)
(cz2168@columbia.edu)
(tln2001@columbia.edu)
(ac1044@columbia.edu)
(vkt2103@columbia.edu)
(djm6@columbia.edu)
(cosmanf@helenhayeshosp.org)
(nievesj@helenhayeshosp.org)
[*]These authors contributed equally to this work.

Author's roles: Study design: XSL, EMS, ES, and XEG. Subject recruitment and data acquisition: EMS, TLN, AC, VT, FC, JN, ES. Data analyses: XSL, EMS, and BZ. Statistical analysis: XSL, CAZ, and DJM. Data interpretation: XSL, EMS, DJM, ES, and XEG. Drafting manuscript: XSL. Revising manuscript content: XSL, EMS, DJM, ES, and XEG. Approval final version of manuscript: XSL, EMS, BZ, CAZ, TLN, AC, VT, DJM, FC, JN, ES, and XEG. XSL takes responsibility for the integrity of the data analyses.

Conflict of Interest: Drs. Liu and Guo are inventors of the ITS analysis software used in the study. All the other authors have no conflicts of interest.

connectivity over rod trabecular parameters, loss of axially aligned trabeculae, and a more rod-like trabecular network. In addition, decreased thickness and size of trabecular plates were observed at the tibia. The differences between groups were greater at the radius than the tibia for plate number, rod bone volume fraction and number and plate-rod and rod-rod junction densities. Most differences between groups remained after adjustment for T-score by DXA. At a fixed bone volume fraction, trabecular plate volume, number and connectivity were directly associated with bone stiffness. In contrast, rod volume, number and connectivity were inversely associated with bone stiffness. In summary, HR-pQCT-based ITS and μFEA measurements discriminate fracture status in postmenopausal women independent of DXA measurements. Moreover, these results suggest that preferential loss of plate-like trabeculae contribute to lower trabecular bone and whole bone stiffness in women with fractures. We conclude that HR-pQCT-based ITS and μFEA measurements increase our understanding of the microstructural pathogenesis of fragility fracture in postmenopausal women.

Keywords

bone micarchitecture; high-resolution peripheral quantitative computed tomography; individual trabecula segmentation; trabecular plate/rod; fragility fractures

INTRODUCTION

Osteoporosis is a common disease of aging in which reduced bone strength leads to increased risk of fracture (1). Pathologically, osteoporosis is characterized by low bone mass, thin porous cortices and decreased trabecular number and connectivity (2,3). Osteoporosis may be diagnosed before fractures occur by measuring areal bone mineral density (aBMD) by dual energy x-ray absorptiometry (DXA) (4). DXA is currently a standard clinical tool for predicting fracture. However, as its resolution is too low to distinguish between the cortical and trabecular compartments or image bone microstructure, DXA is of limited utility in understanding the microarchitectural pathogenesis of fractures or the microarchitectural features of various clinical bone diseases (5–7). Thus, there is great interest in new *in vivo* imaging methods, such as high resolution peripheral quantitative computed tomography (HR-pQCT), which has sufficiently high resolution to image bone microarchitecture (8–10).

Cortical and trabecular bone microstructure can be quantified by the standard analysis software of HR-pQCT (9,10). Moreover, mechanical competence of the whole bone segment and trabecular bone compartment can be estimated by micro finite element analysis (μFEA) (9,11). The accuracy of HR-pQCT and μFEA measurements has been demonstrated in several validation studies (9–11) and these tools have also been utilized in clinical studies to elucidate differences in bone microstructure and mechanical competence between subjects with and without osteoporosis (12,13), and with and without a history of fractures (14–19). In this regard, we have recently reported that (vBMD), microarchitectural deterioration and decreased elastic moduli (20).

The standard analysis of HR-pQCT has two important limitations. First, several parameters are derived rather than directly measured, and are highly interdependent. it does not distinguish between the two different types of trabeculae: plates and Therefore, we have developed a new, rigorous, model-independent 3D morphological analysis tool for HR-pQCT image analysis that yields detailed quantification of trabecular types and direct measurements of each individual trabecula Individual trabecula segmentation (ITS)-based analysis, which segments trabecular microstructure into individual trabecular plates and rods (21,22), has demonstrated trabecular plates and rods of different orientations have distinct

roles in mechanical properties and failure mechanisms of trabecular bone (13,21–23). We have recently that HR-pQCT and ITS distinguish premenopausal women with osteoporosis from controls and detect subtle differences in trabecular plate and rod microstructure groups (24). In a study of skeletal differences between premenopausal Chinese-American and Caucasian women, we found that Chinese-American women have more plate-like trabecular structure but similar rod-like structure to Caucasian women, could account for greater mechanical competence and lower fracture risk in Chinese-American women (25). Additionally, we have also compared ITS measurements of HR-pQCT scans with those of high resolution micro computed tomography (μCT) scans and concluded that HR-pQCT and ITS-based parameters are highly reflective of trabecular bone microarchitecture from a biomechanical perspective (8).

In this study, we compared ITS measures of trabecular microarchitecture and μFEA measures of bone mechanical competence at the distal radius and tibia in postmenopausal women with and without fragility fractures. We hypothesized that ITS and μFEA would discriminate between postmenopausal women with and without fractures independent of aBMD. We also hypothesized that fragility fractures in postmenopausal women are associated with reduced trabecular plate volume and number, a more rod-like structure, and decreased whole bone and trabecular bone stiffness.

Materials and Methods

Patient Population

The current analyses were conducted on the subjects previously described by Stein *et al*. (20). Postmenopausal women, over age 60 or more than 10 years post menopause, were recruited at Columbia University Medical Center (CUMC; New York, NY) or Helen Hayes Hospital (HHH; West Haverstraw, NY) by advertisement, self- or physician referral. Subjects were eligible for inclusion as fracture cases if they had a documented history of a low trauma fracture that occurred after menopause. Low trauma was defined as equivalent to a fall from a standing height or less. Non-vertebral fractures were confirmed by review of radiographs when possible or radiograph report. Vertebral fractures were identified by spine x-rays according to the semi-quantitative method of Genant *et al*. (26). Vertebrae were graded as normal, or with mild, moderate or severe deformities, defined as reductions in anterior, middle or posterior height of 20–25%, 25–40%, and >40% respectively. Control subjects had no history of low trauma fractures and no radiographic vertebral deformities. There were no BMD requirements for inclusion. Potential cases and controls were excluded if they had endocrinopathies (*e.g*., untreated hyperthyroidism, Cushing's syndrome, prolactinoma), celiac disease or other gastrointestinal diseases, abnormal mineral metabolism (*e.g*., osteomalacia, primary hyperparathyroidism), malignancy except for skin cancer, and drug exposures that could affect bone metabolism (*e.g*., glucocorticoids, anticonvulsants, anticoagulants, methotrexate, aromatase inhibitors, thiazolidinediones). Women using hormone replacement therapy or raloxifene were permitted to participate. Women who had ever used teriparatide, or who had taken bisphosphonates for more than one year were excluded. All subjects provided written informed consent and the Institutional Review Boards of CUMC and HHH approved this study.

Of 238 women screened, 169 were eligible and agreed to participate. The most common reasons for exclusion were bisphosphonate use for greater than one year (18%), subject preference not to participate (7%), age < 60 years (5%), glucocorticoid use (3%), primary hyperparathyroidism (2%), bilateral wrist fractures or inability to be properly positioned in the HR-pQCT scanner (2%).

Areal Bone Mineral Density (aBMD)

Areal BMD was measured by DXA (QDR-4500, Hologic Inc., Walton, MA at CUMC; Lunar Prodigy, GE, Peewaukee, WI at HHH) of the lumbar spine (LS), total hip (TH), femoral neck (FN), 1/3 radius (1/3R), and ultradistal radius (UDR). T scores compared subjects and controls with young-normal populations of the same race and sex, as provided by each manufacturer.

HR-pQCT Images of the Distal Radius and Distal Tibia

HR-pQCT (XtremeCT, Scanco Medical AG, Bassersdorf, Switzerland) of the non-dominant distal radius and distal tibia was measured at CUMC as previously described (27–29). The HR-pQCT measurement included 110 slices, corresponding to a 9.02 mm section along the axial direction, with a nominal voxel size of 82 μm. After each scan, a reconstructed slide was examined immediately by the operator. The subjects with severe movement artifact on the first scan were rescanned. The region of interest and representative images of HR-pQCT are shown in Figure 1A. Quality control was provided by scanning the European Forearm Phantom at the time subjects were scanned. The mineralized phase was thresholded according to the standard patient evaluation protocol (30).

Individual Trabecula Segmentation (ITS)-Based Morphological Analyses

The trabecular bone compartment of each HR-pQCT image was manually extracted from cortex (9). All trabecular bone images were then subjected to ITS-based morphological analyses. A complete volumetric decomposition technique was applied to segment the trabecular network into individual plates and rods (21). Briefly, digital topological analysis (DTA)-based skeletonization (31) was applied first to transform a trabecular bone image into a representation composed of surfaces and curves skeleton while preserving the topology (*i.e.*, connectivity, tunnels, and cavities) (32,33) as well as the rod and plate morphology of the trabecular microarchitecture. Then, digital topological classification was applied in which each skeletal voxel was uniquely classified as either a surface or a curve type (34). Using an iterative reconstruction method, each voxel of the original image was classified as belonging to either an individual plate or rod. Based on the 3D evaluations of each individual trabecular plate and rod, bone volume and plate and rod number were evaluated by plate and rod bone volume fraction (pBV/TV and rBV/TV), as well as plate and rod number densities (pTb.N and rTb.N, 1/mm). Plate-to-rod ratio (P-R Ratio), a parameter of plate *versus* rod characteristics of trabecular bone, was defined as plate bone volume divided by rod bone volume. The average size of plates and rods was quantified by plate and rod thickness (pTb.Th and rTb.Th, mm), plate surface area (pTb.S, mm^2), and rod length (rTb.ℓ, mm). Intactness of trabecular network was characterized by plate-plate, plate-rod, and rod-rod junction density (P-P, P-R, and R-R Junc.D, $1/mm^3$), calculated as the total junctions between trabecular plates and rods normalized by the bulk volume. Orientation of trabecular bone network was characterized by axial bone volume fraction (aBV/TV), defined as axially aligned bone volume divided by the bulk volume. The definition of these ITS measurements can be found in Glossary 1 (Supplemental Material). Detailed methods describing the complete volumetric decomposition technique and ITS-based measurements can be found in our recent publications (21,22).

Micro Finite Element Analysis (μFEA)

Each thresholded HR-pQCT whole bone segment image and trabecular bone compartment image of the distal radius and tibia was converted to a μFE model. Bone tissue was modeled as an isotropic, linear elastic material with a Young's modulus (E_s) of 15 GPa and a Poisson's ratio of 0.3 (35). For each model of whole bone or trabecular bone segment, a uniaxial compression test was performed to calculate the reaction force under a

displacement equal to 1% of bone segment height along the axial direction. Whole bone stiffness, defined as reaction force divided by the applied displacement, characterizes the mechanical competence of both cortical and trabecular compartments and is closely related to whole bone strength (11) and fracture risk (19,20,36). Similarly, trabecular bone stiffness characterizes the mechanical competence of trabecular bone compartment. Percent load carried by the cortical compartment at the distal and proximal surface of bone segments was also calculated. All the μFE analyses were performed by using a customized element-by-element pre-conditioned conjugate gradient solver (37).

Statistical Analyses

Analyses were conducted with NCSS software (NCSS 2007, NCSS Statistical Software, Kaysville, Utah) and SAS version 9.1 (SAS Institute Inc., Cary, North Carolina). Two-sided p values <0.05 were considered to indicate statistical significance. Descriptive data are presented as mean ± standard deviation (SD) and group comparisons as mean ± standard error of the mean (SEM). Differences between fracture and non-fracture subjects were assessed by Student's *t* test or Mann-Whitney U test if data was not normally distributed. ANOVA was used to evaluate differences in ITS and μFEA parameters at the radius or tibia after adjustment for aBMD T-score at the ultradistal radius or total hip, respectively. In addition, ANOVA was also used to compare fracture *vs*. non-fracture differences between the radius and tibia, and between plate and rod measurements.

To investigate the contributions of the ITS measurements to mechanical properties of trabecular bone, data from both fracture and non-fracture groups were pooled. Each of the ITS measurements was correlated individually to trabecular bone and whole bone stiffness at the distal radius and tibia. To differentiate the contributions of the ITS measurements to the mechanical properties of trabecular bone from that of bone volume fraction (BV/TV=pBV/TV+rBV/TV), partial correlation analyses between stiffness and ITS measurements with the effect of BV/TV removed were performed. Normality tests of Shapiro Walk, Anderson Darling, and D'Agostino Skewness were performed. Pearson's correlation and partial correlation coefficients were presented if the tested variables passed all the normality tests; otherwise Spearman's correlation and partial correlation coefficients were presented.

Logistic regression analysis was performed to estimate the relative risk of fracture associated with ITS and μFEA parameters by using odds ratios (OR), where fracture status was the dependent variable and ITS and μFEA parameters (all per SD decrease) were the potential predictors. Standard receiver operating characteristic (ROC) curve analysis was also performed to determine the ability of DXA, ITS, and μFEA to discriminate fracture status. In this type of analysis, an area under the curve (AUC) >0.75 is considered compelling evidence for the ability to discriminate an outcome. A diagnostic test with an AUC of 0.5 is considered to perform no better than chance.

Results

Subject Characteristics

Sixty-eight women with a history of postmenopausal fragility fracture and one hundred and one women with no fracture history were enrolled (Table 1). The most common fracture sites were forearm (37%), spine (29%), ankle (19%), metatarsal (16%), and humerus (6%). The average time between symptomatic fracture and evaluation was 6 ± 6 years. Seventeen subjects (25%) had sustained multiple postmenopausal fractures. Subjects were predominantly Caucasian (78%). The groups did not differ according to age, BMI, ethnicity,

years since menopause, chronic medical conditions, osteoporosis risk factors, calcium and vitamin D supplementation, exposure to HRT or bisphosphonates.

Areal Bone Mineral Density by DXA

Mean T scores were above the WHO osteoporosis threshold (T score ≤ −2.5) and did not differ between the groups at the LS, FN, TH and 1/3R (Table 2). At the ultradistal radius, the mean T score was 0.5 SD lower in women with fractures ($p<0.01$; Table 2).

Microarchitecture by ITS analyses

In contrast to the DXA findings, ITS analyses of HR-pQCT images revealed marked differences between fracture and non-fracture subjects (Table 2 and Figure 2). At the radius, plate bone volume fraction and number (pBV/TV and pTb.N) was 30% and 11% lower in fracture subjects, and rod bone volume fraction and number (rBV/TV and rTb.N) was 10% and 5% lower in fracture than non-fracture subjects. The plate to rod ratio (P-R Ratio) was 21% lower in fracture subjects. Junction density measurements (P-P, P-R, and R-R Junc.D), which reflect trabecular network connectivity, were 28%, 25%, and 10% lower at the radius in fracture than non-fracture subjects. However, the size of individual trabecular plates and rods, as assessed by plate and rod thickness (pTb.Th and rTb.Th), plate surface area (pTb.S), and rod length (rTb.ℓ) did not differ by fracture status at the radius. Axial bone volume fraction (aBV/TV) was 22% lower in fracture subjects ($p<0.001$) (Table 2 and Figure 2), indicating that the trabecular bone network was less axially aligned in fracture subjects.

At the tibia, significant differences were mostly observed in plate-related measurements: pBV/TV, pTb.N, P-P Junc.D, P-R Junc.D, P-R Ratio and aBV/TV were 4% to 18% lower in women with fractures, whereas differences in rBV/TV, rTb.N, and R-R Junc.D were not significant. Moreover, pTb.Th and pTb.S were 3% and 5% lower in fracture subjects. However, rTb.Th and rTb.ℓ did not differ by fracture status (Table 2 and Figure 2).

With the exception of R-R Junc.D, all radial ITS parameters remained significantly lower in fracture subjects after controlling for aBMD T-score at the ultradistal radius, the only site at which aBMD differed significantly between groups (Table 2). Similarly, adjustment for aBMD T-score at the total hip did not alter the differences observed in tibial ITS measurements, excepting pTb.S, which was no longer significant.

Several differences between fracture and non-fracture groups were significantly less pronounced at the tibia than radius (rBV/TV, pTb.N, rTb.N, P-R Junc.D, and R-R Junc.D; all $p<0.05$, Figure 2). At the tibia, the percent differences between fracture and non-fracture groups in plate properties (pBV/TV, pTb.N, pTb.Th, P-P Junc.D) were significantly more pronounced than rod properties (rBV/TV, rTb.N, rTb.Th, R-R Junc.D, $p<0.05$). At the radius, the percent difference in pTb.N between fracture and non-fracture groups tended to be greater than the difference in rTb.N ($p=0.07$).

Estimated Stiffness by μFEA

Whole bone and trabecular bone stiffness were lower in women with fractures at both sites (Table 2 and Figure 2). At the radius, whole bone and trabecular bone stiffness were 14% and 34% lower respectively in fracture subjects ($p<0.01$). The between-groups differences were significantly greater ($p<0.05$) at the radius than the tibia, where whole bone and trabecular bone stiffness at the tibia were 11% and 15% lower in women with fractures ($p<0.01$). The percent of load carried by cortex was similar in fracture and non-fracture subjects at both proximal and distal bone surfaces. Trabecular and whole bone stiffness remained significantly lower in fracture subjects at both sites after adjustment for aBMD T-score at the ultradistal radius or total hip.

Logistic Regression Analyses

Odds ratio assessed by logistic regression analysis suggested that aBMD of ultradistal radius, pBV/TV, P-R Ratio, pTb.N, P-P Junc.D, P-R Junc.D, and aBV/TV at both the radius and tibia, rBV/TV, rTb.N, R-R Junc.D at the radius, and pTb.Th at the tibia were significantly associated with the fracture status (Table 2). Each of the SD decrease of the aBMD at the ultradistal radius (OR 1.45; 95% CI, 1.09–1.93) increased the risk of fracture by 45%. The most significant ITS parameters were pBV/TV, aBV/TV, P-P Junc.D and P-R Junc.D (OR 2.08–2.16) at the distal radius such that each SD decrease doubled the risk of fracture. Whole bone and trabecular bone stiffness at both sites were also significantly associated with the fracture status where each of the SD decline increased the risk of fracture by 60~92% (OR 1.60–1.92, Table 2).

By ROC analysis, discrimination of fracture status by DXA, ITS, and μFEA parameters was not statistically different (AUC: 0.51–0.61 for DXA T-score, 0.50–0.70 for ITS of HR-pQCT and μFEA measures, Table 2). Thus, despite the highly significant between-groups differences, no DXA, ITS, or μFEA parameter demonstrated adequate sensitivity or specificity by ROC analysis (AUC >0.75) for fracture status classification. When all parameters were considered together in a multivariable analysis, final models with combined parameters did not improve prediction by a single parameter alone. For example, a multivariable model that included radial pBV/TV and percent cortical load, and tibial pTb.Th and whole bone stiffness, increased AUC from 0.70 to 0.71 for radial aBV/TV alone.

Correlations between ITS and μFEA Parameters

At the radius, all ITS measurements were significantly and positively correlated with whole bone and trabecular bone stiffness, excepting rTb.ℓ, which correlated negatively (Table 3). The tibia resembled the radius with two exceptions; rTb.N did not correlate with trabecular stiffness and R-R Junc.D did not correlate with either whole bone or trabecular bone stiffness (Table 3). At both sites, the strongest correlations were between stiffness and pBV/TV, aBV/TV, pTb.N, P-R Junc.D and P-P Junc.D.

After controlling for BV/TV, correlations between radial ITS parameters (pBV/TV, aBV/TV, P-R Ratio, pTb.N, pTb.Th, rTb.Th, P-P Junc.D, P-R Junc.D) and whole bone and trabecular bone stiffness remained direct and significant. In contrast, rBV/TV, rTb.N, and R-R Junc.D, which were directly related to whole bone and trabecular bone stiffness, became inversely related when the contribution of BV/TV was removed. Results at the tibia were similar, excepting that P-R Junc.D did not correlate with either whole bone or trabecular bone stiffness after controlling for BV/TV.

Discussion

In this study, we found that women with and without a history of postmenopausal fragility fractures had highly significant differences in trabecular microstructure and both whole bone and trabecular bone stiffness at the distal radius and tibia. Characterizing trabecular microstructure at the level of individual trabeculae by ITS revealed that the reductions in trabecular BV/TV and stiffness in women with fractures were associated with lower plate and rod BV/TV, lower plate and rod trabecular number, reduced connectivity between trabecular plates and between trabecular plates and rods, and a less axially aligned trabecular network. The ability of these ITS and μFEA analyses of HR-pQCT scans of the radius and tibia to discriminate fragility fracture status remained significant after adjustment for aBMD T-score by DXA. Moreover, the contribution of these trabecular parameters to stiffness was independent of trabecular BV/TV. To our knowledge, this is the first study to utilize a

model-independent image analysis technique to study microarchitecture of individual trabeculae in women with postmenopausal fragility fractures and their non-fractured peers.

ITS and μFE analyses of HR-pQCT images have been validated for assessing microarchitectural and mechanical properties against the gold standard of micro-computed tomography (8,9,11). In a previous study, in which we performed ITS analyses of HR-pQCT images of normal and osteoporotic premenopausal women, we found that at a fixed bone mass, plate-like trabeculae were directly associated with mechanical properties of trabecular bone (24). Our current study extends previous findings in the same cohort of postmenopausal women previously reported by Stein *et al.*; by HR-pQCT, those with a history of fracture had lower vBMD, thinner cortices, and thinner trabeculae at both radius and tibia, and fewer, more widely and unevenly spaced trabeculae at the distal radius (20). The ITS and μFE data reported here provide further mechanistic insights into these trabecular microarchitectural differences, and suggest that preferential loss of plate bone volume, plate number, and plate-plate junction density lead to a more rod-like and less axially aligned trabecular network and decreased trabecular bone stiffness in women with fractures. We also found that women with a history of fractures had significantly lower whole bone stiffness at both sites compared to controls, although the percent load carried by cortical versus trabecular bone did not differ. Therefore, from a biomechanical perspective, women with fragility fractures had comparable deterioration in both cortical and trabecular bone compartments.

Several studies have used HR-pQCT patient-standard analyses to evaluate bone microstructure in postmenopausal women with and without fractures (19,20,29,36,38). Stein *et al.* (20) and Sornay-Rendu *et al.* (29) studied subjects with a variety of central and peripheral fractures, finding decreased BV/TV^d and trabecular thickness (Tb.Th) at the radius and tibia, and decreased trabecular number (Tb.N*) and increased trabecular spacing (Tb.Sp) at the radius. Our results provide further clarification of different patterns of trabecular loss at the radius and tibia. The decreased radius BV/TV^d and Tb.N* in fracture group appears to be due to loss of both plates and rods. At the tibia, Tb.N* by HR-pQCT standard analysis did not differ between the fracture and non-fracture groups. However, ITS analyses revealed preferential loss of trabecular plates in the fractured subjects and no difference in rod parameters. Tb.Th and Tb.Sp were not model-independent measurements but rather derived from BV/TV^d and Tb.N*; however, they were significantly correlated to pTb.Th and rTb.Th, and rTb.ℓ, respectively (data not shown). At the radius, the decrease in Tb.Th in fracture subjects corresponded to a decrease in pTb.Th, and the increase in Tb.Sp was consistent with an increase in rTb.ℓ ($p=0.051$).

Few studies have described the differences in whole bone stiffness or strength parameters by HR-pQCT-based μFEA between women with and without fractures. Melton *et al.* reported a significant reduction in the estimated failure load at the radius in postmenopausal women with forearm fractures versus controls (36). Similarly, Vilayphiou *et al.* reported that estimated bone stiffness of both radius and tibia was significantly lower in postmenopausal women with various types of fractures than non-fractured controls (19). Our results are consistent with these studies. Vilayphiou *et al.* also found that the percent load carried by cortex at the distal surface of the radius was significantly greater in women with fractures (19) while Melton et al. found the percent load carried by cortex was similar in women with or without wrist fractures (36). We found no significant difference in the percent cortical load between fracture and non-fracture groups.

In our previous report using the standard HR-pQCT patient analysis in these same women (20), as well as in the study by Sornay-Rendu et al. (29), fracture subjects had greater alterations in trabecular microarchitecture at the radius than tibia. Our current study extends

these previous findings, confirming that differences in several ITS and μFEA parameters between women with and without fractures were more apparent at the radius than tibia. One explanation is that weight-bearing may attenuate the differences at the distal tibia. An alternative explanation may relate to the predominance of vertebral and wrist fractures in our study and the study of Sornay-Rendu *et al.* (29). In this regard, we recently measured volumetric density and mechanical competence at the radius, tibia, lumbar spine and proximal femur by HR-pQCT, central QCT (cQCT) and FEA, finding that HR-pQCT of the radius was more strongly associated with stiffness at the forearm and spine, while HR-pQCT of the tibia was more strongly associated with stiffness at the hip (39). These results are consistent with those of Sornay-Rendu *et al*. and suggest that microstructural parameters at the radius are more strongly associated with number and severity of postmenopausal vertebral fractures than those at the tibia (40). Similarly, Stein *et al*. demonstrated that differences in bone microarchitecture and bone stiffness between women with ankle fractures and controls were more pronounced at the tibia (38), and Vico *et al*. reported that tibial trabecular microarchitectural deterioration was more severe in women with hip fractures than those with wrist fractures (41). Therefore, the ability of measurements at peripheral sites to discriminate fracture status may differ by fracture type.

In contrast to the major differences between fractured and non-fractured women detected by ITS and μFE analyses of HR-pQCT, by DXA only UDR aBMD T-score differed significantly, with no differences were detected at any of the sites typically used for diagnosis of osteoporosis. Although the AUC for several ITS and μFE parameters (0.69–0.70) were higher than those for DXA (0.51–0.62), none achieved sufficient sensitivity or specificity for fracture discrimination (AUC<0.75). In addition, the AUC for vBMD and standard microarchitectural parameters as assessed by HR-pQCT (0.55–0.67) reported by Stein et al., were comparable with the AUC for ITS and μFE parameters; no imaging modality had an AUC for fracture prediction >0.75. This suggests that accounting for other fracture risk factors, such as muscle strength, balance, and propensity for falls, is essential to improve the sensitivity and specificity for fracture status discrimination and fracture prediction. However, HR-pQCT-based ITS and μFEA provide unique mechanistic insights into differences in bone microarchitecture and strength that may predispose to fracture.

This study has several limitations. The cross-sectional study design precludes us from determining whether HR-pQCT-based ITS and μFEA predict incident fractures. A longitudinal study would be necessary to determine whether ITS can predict fracture. Furthermore, ITS analysis in longitudinal studies may provide more detailed information on changes in trabecular bone with progression of osteoporosis or with pharmacological interventions. Indeed, an ITS application in a longitudinal micro magnetic resonance imaging (μMRI) study of osteoporotic hypogonadal men with 24 months testosterone treatment has demonstrated the potential of ITS in detecting important microstructural changes in osteoporosis and its treatment (42). Input images for ITS-based analyses were thresholded by the global threshold technique provided by the HR-pQCT manufacturer, which overestimates trabecular bone volume, number, and thickness (8,9). The limited spatial resolution and signal-to-noise ratio of HR-pQCT influenced the accuracy of ITS measurements, especially the junction densities measurements (8). As cortical and trabecular bone tissue were assumed to be constant and homogeneous for all the subjects, current μFE-based analyses reflect bone microstructure but not tissue properties, such as collagen cross-link and degree of mineralization that may be associated with postmenopausal osteoporosis. In future, it may be possible to derive tissue properties from HR-pQCT images and integrate them into μFE analyses. In the current study, subjects with fractures of different types were included and analyzed as a group. The number of subjects was too small to assess whether specific differences in trabecular bone microarchitecture are associated with different types of fractures.

In conclusion, ITS analysis of HR-pQCT images detected marked differences in plate and rod trabecular microarchitecture between postmenopausal women with peripheral and central fragility fractures and those without fractures independent of aBMD by DXA. The most consistent finding was a preferential reduction in the volume, number, and connectivity of trabecular plates over rods, loss of axially aligned trabeculae, and a more rod-like trabecular network. Decreased thickness and size of trabecular plates was additionally observed at the tibia. Interestingly, this pattern differed from that reported in premenopausal women with osteoporosis, which was characterized by similar reductions in both plate-and rod-like trabecular microstructure without alterations in plate or rod thickness (24). At a fixed bone volume fraction, the volume, number, and connectivity of plates were positively associated with bone stiffness while the corresponding rod parameters were negatively associated with bone stiffness. Our findings suggest that preferential loss of plate-like trabeculae exacerbate reduced bone stiffness in postmenopausal women with fractures. These novel *in vivo* microstructural and mechanical measurements shed light on differences in bone quality associated with postmenopausal fragility fracture risk.

Supplementary Material

Refer to Web version on PubMed Central for supplementary material.

Acknowledgments

This work was supported by NIH Grants R01 AR051376 (XEG), NIH R01 AR058004 (XEG, ES), NIH U01 AR055968 (ES), NIH K23 DK084337 (EMS) and by the Thomas L. Kempner and Katheryn C. Patterson Foundation.

Reference

1. NIH Consensus Development Panel on Osteoporosis Prevention. Consensus Development Conference Report: Prophylaxis and treatment of osteoporosis. Osteoporosis Int. 1991; 1(2):114–7.
2. Genant HK, Delmas PD, Chen P, Jiang Y, Eriksen EF, Dalsky GP, Marcus R, San Martin J. Severity of vertebral fracture reflects deterioration of bone microarchitecture. Osteoporos Int. 2007; 18(1):69–76. [PubMed: 17028792]
3. Qiu S, Rao DS, Palnitkar S, Parfitt AM. Independent and combined contributions of cancellous and cortical bone deficits to vertebral fracture risk in postmenopausal women. J Bone Miner Res. 2006; 21(11):1791–6. [PubMed: 17002584]
4. Miller, PD. Clinical use of bone mass measurements in adults for the assessment and management of osteoporosis. In: Favus, MJ., editor. Primer on the Metabolic Bone Disease and Disorders of Mineral Metabolism. 6th ed.. American Society for Bone and Mineral Research; Washington DC: 2006. p. 150-61.
5. Hui SL, Slemenda CW, Johnston CC Jr. Age and bone mass as predictors of fracture in a prospective study. Journal of Clinical Investigation. 1988; 81(6):1804–9. [PubMed: 3384952]
6. Siris ES, Miller PD, Barrett-Connor E, Faulkner KG, Wehren LE, Abbott TA, Berger ML, Santora AC, Sherwood LM. Identification and fracture outcomes of undiagnosed low bone mineral density in postmenopausal women: results from the National Osteoporosis Risk Assessment. Jama. 2001; 286(22):2815–22. [PubMed: 11735756]
7. Schuit SC, van der Klift M, Weel AE, de Laet CE, Burger H, Seeman E, Hofman A, Uitterlinden AG, van Leeuwen JP, Pols HA. Fracture incidence and association with bone mineral density in elderly men and women: the Rotterdam Study. Bone. 2004; 34(1):195–202. [PubMed: 14751578]
8. Liu XS, Shane E, McMahon DJ, Guo XE. Individual trabecula segmentation (ITS)-based morphological analysis of micro-scale images of human tibial trabecular bone at limited spatial resolution. J Bone Miner Res. 2011; 26(9):2184–93. [PubMed: 21557311]

9. Liu XS, Zhang XH, Sekhon KK, Adams MF, McMahon DJ, Bilezikian JP, Shane E, Guo XE. High-resolution peripheral quantitative computed tomography can assess microstructural and mechanical properties of human distal tibial bone. J Bone Miner Res. 2010; 25(4):746–56. [PubMed: 19775199]
10. MacNeil JA, Boyd SK. Accuracy of high-resolution peripheral quantitative computed tomography for measurement of bone quality. Med Eng Phys. 2007; 29(10):1096–105. [PubMed: 17229586]
11. Macneil JA, Boyd SK. Bone strength at the distal radius can be estimated from high-resolution peripheral quantitative computed tomography and the finite element method. Bone. 2008; 42(6): 1203–13. [PubMed: 18358799]
12. Cohen A, Liu XS, Stein EM, McMahon DJ, Rogers HF, Lemaster J, Recker RR, Lappe JM, Guo XE, Shane E. Bone microarchitecture and stiffness in premenopausal women with idiopathic osteoporosis. J Clin Endocrinol Metab. 2009; 94(11):4351–60. [PubMed: 19837923]
13. Liu XS, Bevill G, Keaveny TM, Sajda P, Guo XE. Micromechanical analyses of vertebral trabecular bone based on individual trabeculae segmentation of plates and rods. J Biomech. 2009; 42(3):249–56. [PubMed: 19101672]
14. Boutroy S, Van Rietbergen B, Sornay-Rendu E, Munoz F, Bouxsein ML, Delmas PD. Finite element analysis based on in vivo HR-pQCT images of the distal radius is associated with wrist fracture in postmenopausal women. J Bone Miner Res. 2008; 23(3):392–9. [PubMed: 17997712]
15. Melton LJ 3rd, Riggs BL, Keaveny TM, Achenbach SJ, Hoffmann PF, Camp JJ, Rouleau PA, Bouxsein ML, Amin S, Atkinson EJ, Robb RA, Khosla S. Structural determinants of vertebral fracture risk. J Bone Miner Res. 2007; 22(12):1885–92. [PubMed: 17680721]
16. Melton LJ 3rd, Riggs BL, van Lenthe GH, Achenbach SJ, Muller R, Bouxsein ML, Amin S, Atkinson EJ, Khosla S. Contribution of in vivo structural measurements and load/strength ratios to the determination of forearm fracture risk in postmenopausal women. J Bone Miner Res. 2007; 22(9):1442–8. [PubMed: 17539738]
17. Melton LJ 3rd, Christen D, Riggs BL, Achenbach SJ, Muller R, van Lenthe GH, Amin S, Atkinson EJ, Khosla S. Assessing forearm fracture risk in postmenopausal women. Osteoporos Int. 2009
18. Vilayphiou N, Boutroy S, Sornay-Rendu E, Van Rietbergen B, Munoz F, Delmas PD, Chapurlat R. Finite element analysis performed on radius and tibia HR-pQCT images and fragility fractures at all sites in postmenopausal women. Bone.
19. Vilayphiou N, Boutroy S, Sornay-Rendu E, Van Rietbergen B, Munoz F, Delmas PD, Chapurlat R. Finite element analysis performed on radius and tibia HR-pQCT images and fragility fractures at all sites in postmenopausal women. Bone. 2010; 46(4):1030–7. [PubMed: 20044044]
20. Stein EM, Liu XS, Nickolas TL, Cohen A, Thomas V, McMahon DJ, Zhang C, Yin PT, Cosman F, Nieves J, Guo XE, Shane E. Abnormal microarchitecture and reduced stiffness at the radius and tibia in postmenopausal women with fractures. J Bone Miner Res. 2010; 25(12):2296–305.
21. Liu XS, Sajda P, Saha PK, Wehrli FW, Bevill G, Keaveny TM, Guo XE. Complete volumetric decomposition of individual trabecular plates and rods and its morphological correlations with anisotropic elastic moduli in human trabecular bone. J Bone Miner Res. 2008; 23(2):223–35. [PubMed: 17907921]
22. Liu XS, Sajda P, Saha PK, Wehrli FW, Guo XE. Quantification of the roles of trabecular microarchitecture and trabecular type in determining the elastic modulus of human trabecular bone. J Bone Miner Res. 2006; 21(10):1608–17. [PubMed: 16995816]
23. Fields AJ, Lee GL, Liu XS, Jekir MG, Guo XE, Keaveny TM. Influence of vertical trabeculae on the compressive strength of the human vertebra. J Bone Miner Res. 2011; 26(2):263–9. [PubMed: 20715186]
24. Liu XS, Cohen A, Shane E, Stein E, Rogers HF, Kokolus SL, Yin PT, McMahon DJ, Lappe JM, Recker RR, Guo XE. Individual trabeculae segmentation (ITS)-based morphological analyses of high resolution peripheral quantitative computed tomography images detect abnormal trabecular plate and rod microarchitecture in premenopausal women with idiopathic osteoporosis. J Bone Miner Res. 2010; 25(7):1486–1505.
25. Liu XS, Walker MD, McMahon DJ, Udesky J, Liu G, Bilezikian JP, Guo XE. Better skeletal microstructure confers greater mechanical advantages in Chinese-American women versus Caucasian women. J Bone Miner Res. 2011; 26(8):1783–92. [PubMed: 21351150]

26. Genant HK, Wu CY, van Kuijk C, Nevitt MC. Vertebral fracture assessment using a semiquantitative technique. J Bone Miner Res. 1993; 8(9):1137–48. [PubMed: 8237484]
27. Boutroy S, Bouxsein ML, Munoz F, Delmas PD. In vivo assessment of trabecular bone microarchitecture by high-resolution peripheral quantitative computed tomography. J Clin Endocrinol Metab. 2005; 90(12):6508–15. [PubMed: 16189253]
28. Boutroy S, van Rietbergen B, Sornay-Rendu E, Munoz F, Bouxsein ML, Delmas PD. Finite Element Analyses Based on In Vivo HR-pQCT Images of the Distal Radius is Associated with Wrist Fracture in Postmenopausal Women. J Bone Miner Res. 2008; 23(3):392–9. [PubMed: 17997712]
29. Sornay-Rendu E, Boutroy S, Munoz F, Delmas PD. Alterations of cortical and trabecular architecture are associated with fractures in postmenopausal women, partially independent of decreased BMD measured by DXA: the OFELY study. J Bone Miner Res. 2007; 22(3):425–33. [PubMed: 17181395]
30. Laib A, Hauselmann HJ, Ruegsegger P. In vivo high resolution 3D-QCT of the human forearm. Technol Health Care. 1998; 6(5–6):329–37. [PubMed: 10100936]
31. Saha PK, Chaudhuri BB, Majumder DD. A new shape preserving parallel thinning algorithm for 3D digital images. Pattern Recogn. 1997; 30(12):1939–55.
32. Saha PK, Chaudhuri BB. Detection of 3-D simple points for topology preserving. IEEE Trans Pattern Anal Mach Intell. 1994; 16(10):1028–32.
33. Saha PK, Chaudhuri BB, Chanda B, Dutta Majumder D. Topology preservation in 3D digital space. Pattern Recogn. 1994; 27:295–300.
34. Saha PK, Chaudhuri BB. 3D digital topology under binary transformation with applications. Comput Vis Image Underst. 1996; 63(3):418–29.
35. Guo XE, Goldstein SA. Is trabecular bone tissue different from cortical bone tissue? Forma. 1997; 12:185–96.
36. Melton LJ 3rd, Christen D, Riggs BL, Achenbach SJ, Muller R, van Lenthe GH, Amin S, Atkinson EJ, Khosla S. Assessing forearm fracture risk in postmenopausal women. Osteoporos Int. 2010; 21(7):1161–9. [PubMed: 19714390]
37. Hollister SJ, Brennan JM, Kikuchi N. A homogenization sampling procedure for calculating trabecular bone effective stiffness and tissue level stress. J Biomech. 1994; 27(4):433–44. [PubMed: 8188724]
38. Stein EM, Liu XS, Nickolas TL, Cohen A, Thomas V, McMahon DJ, Zhang C, Cosman F, Nieves J, Greisberg J, Guo XE, Shane E. Abnormal Microarchitecture and Stiffness in Postmenopausal Women with Ankle Fractures. J Clin Endocrinol Metab. 2011; 96(7):2041–8. [PubMed: 21508142]
39. Liu XS, Cohen A, Shane E, Yin PT, Stein EM, Rogers H, Kokolus SL, McMahon DJ, Lappe JM, Recker RR, Lang T, Guo XE. Bone density, geometry, microstructure and stiffness: relationships between peripheral and central skeletal sites assessed by DXA, HR-pQCT, and cQCT in premenopausal women. J Bone Miner Res. 2010; 25(10):2229–38. [PubMed: 20499344]
40. Sornay-Rendu E, Cabrera-Bravo JL, Boutroy S, Munoz F, Delmas PD. Severity of vertebral fractures is associated with alterations of cortical architecture in postmenopausal women. J Bone Miner Res. 2009; 24(4):737–43. [PubMed: 19113929]
41. Vico L, Zouch M, Amirouche A, Frere D, Laroche N, Koller B, Laib A, Thomas T, Alexandre C. High-resolution pQCT analysis at the distal radius and tibia discriminates patients with recent wrist and femoral neck fractures. J Bone Miner Res. 2008; 23(11):1741–50. [PubMed: 18665795]
42. Zhang XH, Liu XS, Vasilic B, Wehrli FW, Benito M, Rajapakse CS, Snyder PJ, Guo XE. In vivo μMRI based finite element and morphological analyses of tibial trabecular bone in eugonadal and hypogonadal men before and after testosterone treatment. J Bone Miner Res. 2008; 23(9):1426–34. [PubMed: 18410234]

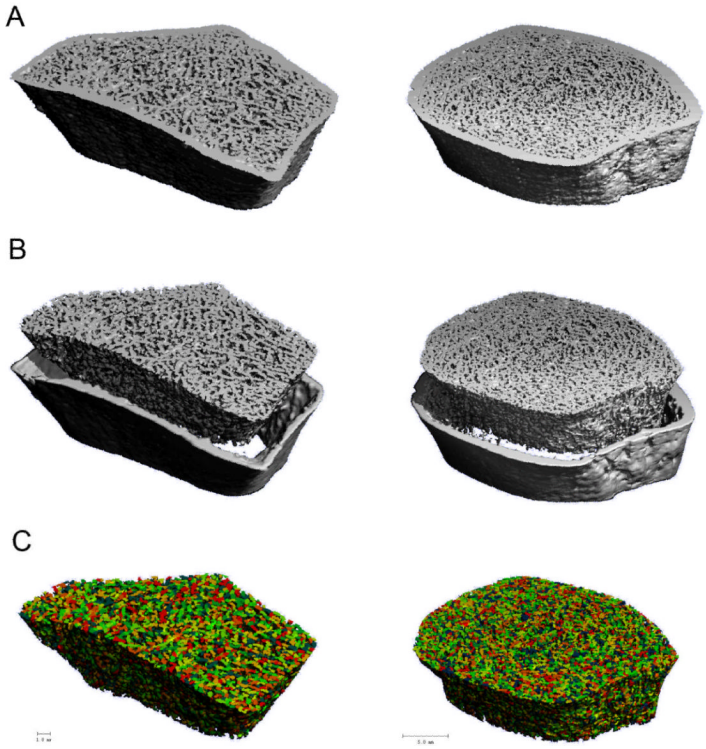

Figure 1.
Based on the (A) 3D reconstructed HR-pQCT images of the distal radius (Left) and tibia (Right), (B) trabecular bone compartments were first segmented from cortex, and then (C) subjected to ITS analyses for a decomposition of individual trabecular plates and rods (Different color indicate different individual trabecula).

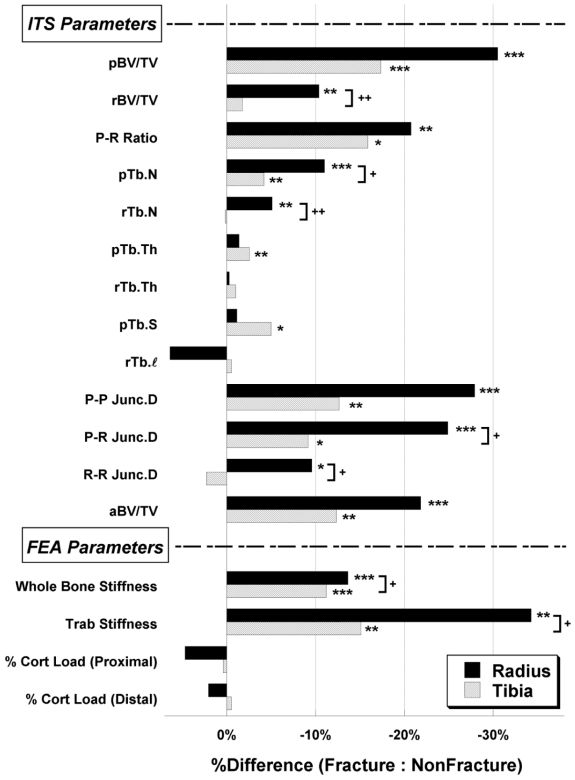

Figure 2.

Comparisons of percent difference in HR-pQCT-based ITS and μFEA measurements between fracture and nonfracture subjects at the distal radius (filled bars) and tibia (open bars). *p<0.05, **p<0.01, ***p<0.001 for comparisons between fracture and nonfracture subjects; $^{+}p<0.05$, $^{++}p<0.01$ for comparisons between radius and tibia.

Table 1

Characteristics of the study population (mean ± SEM)

	Fracture N=68	Non-fracture N=101	P-value
Age (years)	69 ± 1	68 ± 1	0.30
Race % Caucasian	81%	76%	0.93
% African American	3%	5%	
% Hispanic	15%	17%	
% Other	1%	2%	
Height (cm)	160 ± 1	161 ± 1	0.36
Weight (kg)	67 ± 2	68 ± 2	0.60
Years since menopause	20 ± 1	18 ± 1	0.34
Oophorectomy (%)	18%	18%	0.99
Family history of osteoporosis (%)	49%	44%	0.63
Family history of fracture (%)	38%	36%	0.87
Tobacco use –Pack years	22 ± 5	21 ± 3	0.85
Never (%)	50%	44%	
Former (%)	50%	54%	
Current (%)	0%	1%	
Alcohol use (beverages per day)	1 ± 0	1 ± 0	0.99
Medication Use			
Calcium supplements – total daily dose (mg)	608 ± 78	612 ± 60	0.97
Vitamin D supplements – total daily dose (IU)	568 ± 78	797 ± 135	0.19
Hormone replacement therapy – Past (%)	42%	46%	0.87
Current (%)	3%	6%	0.67
Bisphosphonates - Past (%)	6%	5%	0.99
Current (%)	4%	1%	0.46
Raloxifene (%)	6%	2%	0.37
Thyroxine (%)	8%	22%	0.02

Table 2

Comparison of DXA, ITS and mechanical parameters in subjects with and without fractures. Letters denote significance of comparisons after adjustment for UDR (radius) and TH (tibia) T-score.

Variable (units)	Fracture (Mean ± SEM)	Nonfracture (Mean ± SEM)	p Value	OR (95%CI)	AUC
DXA T-Score					
Total Spine	−1.32 ± 0.16	−1.26 ± 0.14	0.87	1.03 (0.82, 1.29)	0.51
Total Hip	−1.25 ± 0.11	−1.16 ± 0.10	0.54	1.11 (0.80, 1.54)	0.52
Femoral Neck	−1.77 ± 0.08	−1.67 ± 0.08	0.66	1.18 (0.79, 1.77)	0.52
1/3 Radius	−1.43 ± 0.15	−1.32 ± 0.12	0.58	1.07 (0.83, 1.38)	0.51
Ultradistal Radius	−1.65 ± 0.12	−1.15 ± 0.13	0.008	1.45 (1.09, 1.93)*	0.61
ITS – Radius					
BV/TV	0.194 ± 0.006	0.232 ± 0.006	<0.0001[c]	2.15 (1.47, 3.15)*	0.69
pBV/TV	0.049 ± 0.003	0.070 ± 0.004	<0.0001[b]	2.08 (1.41, 3.07)*	0.68
rBV/TV	0.145 ± 0.004	0.162 ± 0.003	0.002[a]	1.67 (1.19, 2.36)*	0.62
P-R Ratio	0.343 ± 0.023	0.433 ± 0.022	0.006[a]	1.62 (1.13, 2.32)*	0.63
pTb.N (1/mm)	1.156 ± 0.028	1.298 ± 0.022	<0.0001[b]	1.96 (1.37, 2.81)*	0.68
rTb.N (1/mm)	1.720 ± 0.024	1.813 ± 0.016	0.001[a]	1.71 (1.22, 2.40)*	0.63
pTb.Th (mm)	0.203 ± 0.001	0.206 ± 0.001	0.09	1.32 (0.95, 1.84)	0.59
rTb.Th (mm)	0.214 ± 0.001	0.215 ± 0.001	0.71	1.06 (0.77, 1.46)	0.57
pTb.S (mm^2)	0.141 ± 0.003	0.143 ± 0.003	0.7	1.06 (0.77, 1.47)	0.54
rTb.l (mm)	0.741 ± 0.020	0.696 ± 0.010	0.051	0.70 (0.48, 1.01)	0.66
P-P Junc.D ($1/mm^3$)	1.003 ± 0.060	1.391 ± 0.064	<0.0001[b]	2.16 (1.45, 3.20)*	0.69
P-RJunc.D ($1/mm^3$)	2.240 ± 0.117	2.982 ± 0.121	<0.0001[b]	2.16 (1.45, 3.20)*	0.69
R-RJunc.D ($1/mm^3$)	2.578 ± 0.091	2.851 ± 0.074	0.02	1.46 (1.05, 2.02)*	0.59
aBV/TV	0.064 ± 0.003	0.082 ± 0.003	<0.0001[c]	2.14 (1.46, 3.16)*	0.70
FEA – Radius					
Whole Bone Stiffness (N/mm)	60502 ± 1579	70048 ± 1876	0.0001[a]	1.92 (1.31, 2.81)*	0.66

Variable (units)	Fracture (Mean ± SEM)	Nonfracture (Mean ± SEM)	p Value	OR (95%CI)	AUC
Trabecular Bone Stiffness (N/mm)	6949 ± 817	10573 ± 834	0.003[a]	1.73 (1.18, 2.52)*	0.65
Cortical Load (%) –Distal	42.8 ± 1.3	40.9 ± 0.9	0.21	0.82 (0.60, 1.12)	0.56
Cortical Load (%) –Proximal	92.2 ± 0.9	90.4 ± 0.7	0.1	0.76 (0.55, 1.05)	0.58
ITS–Tibia					
BV/TV	0.238 ± 0.005	0.261 ± 0.004	0.001[c]	1.75 (1.23, 2.49)*	0.63
pBV/TV	0.094 ± 0.004	0.114 ± 0.004	0.0006[c]	1.82 (1.28, 2.60)*	0.65
rBV/TV	0.144 ± 0.004	0.147 ± 0.003	0.61	1.09 (0.79, 1.49)	0.53
P-R Ratio	0.692 ± 0.038	0.822 ± 0.036	0.02[a]	1.51 (1.07, 2.13)*	0.61
pTb.N (1/mm)	1.419 ± 0.016	1.482 ± 0.014	0.005[b]	1.60 (1.14, 2.24)*	0.63
rTb.N (1/mm)	1.764 ± 0.020	1.760 ± 0.017	0.9	0.98 (0.72, 1.34)	0.50
pTb.Th (mm)	0.213 ± 0.001	0.219 ± 0.001	0.001[b]	1.81 (1.24, 2.62)*	0.65
rTb.Th (mm)	0.216 ± 0.001	0.218 ± 0.001	0.11	1.32 (0.91, 1.90)	0.56
pTb.S (mm^2)	0.148 ± 0.002	0.156 ± 0.003	0.049	1.69 (0.97, 2.95)	0.58
rTb.l (mm)	0.664 ± 0.003	0.667 ± 0.008	0.66	1.07 (0.75, 1.52)	0.48
P-P Junc.D ($1/mm^3$)	1.684 ± 0.052	1.927 ± 0.050	0.001[c]	1.74 (1.23, 2.48)*	0.63
P-R Junc.D ($1/mm^3$)	3.210 ± 0.086	3.534 ± 0.085	0.01[b]	1.54 (1.10, 2.16)*	0.60
R-R Junc.D ($1/mm^3$)	2.506 ± 0.100	2.450 ± 0.082	0.66	0.93 (0.68, 1.27)	0.52
aBV/TV	0.099 ± 0.003	0.113 ± 0.003	0.001[c]	1.76 (1.24, 2.49)*	0.65
FEA – Tibia					
Whole Bone Stiffness	182801 ± 4607	205852 ± 4396	0.0006[d]	1.81 (1.27, 2.59)*	0.64
Trab Stiffness	68975 ± 3092	81741 ± 3233	0.005[b]	1.60 (1.12, 2.28)*	0.62
Cortical Load (%) –Distal	26.3 ± 1.1	26.2 ± 0.8	0.94	0.99 (0.72, 1.35)	0.50
Cortical Load (%) –Proximal	68.9 ± 1.2	69.2 ± 0.9	0.8	1.04 (0.76, 1.42)	0.52

OR: odds ratio per SD decrease; Asterisks denote significant association with fracture status. AUC: area under the receiver operator characteristic (ROC) curve.

[a] $p<0.05$

[b] $p<0.01$

[c] $p<0.001$

[d] $p<0.0001$

Table 3

Correlation coefficient of linear regression and partial correlation coefficient (independent of BV/TV, shown in parentheses) of ITS measurements with whole bone and trabecular bone stiffness of HR-pQCT images at both the distal radius and tibia.

	Distal Radius		Distal Tibia	
	Trabecular Bone Stiffness	**Whole Bone Stiffness**	**Trabecular Bone Stiffness**	**Whole Bone Stiffness**
BV/TV	**0.84** ^{d}	**0.71** ^{d}	**0.74** ^{d}	**0.76** ^{d}
pBV/TV	**0.83**^{d} (**0.43**^{d})	**0.64**^{d} (0.19^{a})	**0.72**^{d} (**0.42**^{d})	**0.68**^{d} (**0.32**^{d})
rBV/TV	**0.49**^{d} (−**0.48**^{d})	**0.48**^{d} (−**0.27**^{b})	0.18^{a} (−**0.34**^{d})	0.22^{b} (−0.25^{b})
P-R Ratio	**0.67**^{d} (**0.42**^{d})	**0.52**^{d} (0.22^{b})	**0.46**^{d} (**0.40**^{d})	**0.40**^{d} (**0.30**^{d})
pTb.N (1/mm)	**0.83**^{d} (**0.35**^{d})	**0.67**^{d} (0.21^{b})	**0.78**^{d} (**0.44**^{d})	**0.72**^{d} (**0.31**^{d})
rTb.N (1/mm)	**0.46**^{d} (−**0.43**^{d})	**0.39**^{d} (−0.21^{b})	0.08 (−**0.44**^{d})	0.16^{a} (−0.22^{b})
pTb.Th (mm)	**0.60**^{d} (**0.36**^{d})	**0.45**^{d} (0.17^{a})	**0.37**^{d} (0.20^{b})	**0.37**^{d} (0.23^{b})
rTb.Th (mm)	**0.53**^{d} (**0.46**^{d})	**0.46**^{d} (**0.33**^{d})	**0.41**^{d} (**0.47**^{d})	**0.26**^{c} (0.22^{b})
pTb.S (mm^{2})	**0.40**^{d} (**0.42**^{d})	0.25^{b} (0.16^{a})	0.22^{b} (**0.32**^{d})	0.17^{a} (0.24^{b})
rTb.ℓ (mm)	−**0.73**^{d} (0.06)	−**0.62**^{c} (−0.07)	−**0.47**^{d} (0.06)	−**0.48**^{d} (0.03)
P-P Junc.D (1/mm^{3})	**0.87**^{d} (**0.46**^{d})	**0.71**^{d} (**0.27**^{c})	**0.80**^{d} (**0.48**^{d})	**0.73**^{d} (**0.28**^{c})
P-R Junc.D (1/mm^{3})	**0.83**^{d} (0.18^{a})	**0.73**^{d} (0.24^{b})	**0.70**^{d} (0.07)	**0.65**^{d} (−0.02)
R-R Junc.D (1/mm^{3})	**0.33**^{d} (−**0.41**^{d})	**0.36**^{d} (−**0.29**^{c})	−0.01 (−0.38^{d})	0.06 (−0.24^{b})
aBV/TV	**0.89**^{d} (**0.55**^{d})	**0.69**^{d} (0.25^{b})	**0.76**^{d} (**0.50**^{d})	**0.69**^{d} (**0.33**^{d})

Significant correlations after adjustment for multiple comparisons are highlighted in bold (p<0.001). Data was combined from both fracture and non-fracture groups.

^{a}p<0.05

^{b}p<0.01

^{c}p<0.001

^{d}p<0.0001.